Journal of Advanced Ceramics
2018, **7**(2): 160–168
https://doi.org/10.1007/s40145-018-0267-3
ISSN 2226-4108
CN 10-1154/TQ

Research Article

Synthesis, sintering, and thermoelectric properties of the solid solution $La_{1-x}Sr_xCoO_{3\pm\delta}$ ($0 \leqslant x \leqslant 1$)

M. A. BOUSNINA[a], R. DUJARDIN[a], L. PERRIERE[b], F. GIOVANNELLI[a], G. GUEGAN[c], F. DELORME[a,*]

[a]*Université François Rabelais de Tours, CNRS, INSA CVL, GREMAN UMR7347, IUT de Blois, 15 rue de la chocolaterie, CS2903, F-41029 Blois Cedex, France*
[b]*ICMPE, 2-8 Rue Henri Dunant, 94320 Thiais, France*
[c]*ST Microelectronics, 16 Rue Pierre et Marie Curie, 37100 Tours, France*

Received: December 21, 2017; Revised: March 5, 2018; Accepted: March 9, 2018

Abstract: In this work, we synthesized cubic perovskite ceramics of the whole $La_{1-x}Sr_xCoO_3$ ($0 \leqslant x \leqslant 1$) solid solution for the first time. Synthesis was carried out by solid state reaction and conventional sintering to reach dense ceramics. For $x > 0.8$, it was necessary to substitute 3% cobalt by silicon to stabilize the cubic perovskite structure. Electrical conductivity increased with Sr content to reach 3×10^5 S·m^{-1} at 330 K for $x = 0.3$. However, the optimum electrical properties have been found for $x = 0.05$ at 330 K with $PF_{max} = 3.11\times10^{-4}$ W·m^{-1}·K^{-2}. Indeed, the Seebeck coefficient was decreasing when x increased to reach values close to 0 for $x \geqslant 0.3$. Thermal conductivity was low at low temperature ($\approx$ 2.5 W·m^{-1}·K^{-1}) and increased up to 6.5 W·m^{-1}·K^{-1} when temperature increased. As the highest power factor was reached at low temperature as well as the lowest thermal conductivity, $La_{1-x}Sr_xCoO_3$ compounds with low x values appeared as very promising thermoelectric materials around room temperature, on the contrary to layered cobalt oxides. For high x values, Seebeck coefficient values close to zero made these materials unsuitable for thermoelectric applications.

Keywords: perovskite; cobalt oxide; solid solution; electrical conductivity; thermoelectric

1 Introduction

In recent years, considerable effort has been devoted to thermoelectricity because of rising cost of energy and environmental requirements. Indeed, thermoelectric converters can convert directly the dissipated heat into electricity with zero emission (CO_2, other gases, radiation, etc.), and without vibration. The thermoelectric performance of a material can be assessed by the figure of merit, $ZT = S^2\sigma T/\kappa$, where S, σ, T, and κ represent the Seebeck coefficient, electrical conductivity, absolute temperature, and thermal conductivity, respectively. The numerator ($S^2\sigma$) is related to electric power for thermoelectric generation and is referred as the power factor (PF). Therefore, in order to achieve a good thermoelectric material, high Seebeck coefficient and high electrical conductivity, leading to a high PF, have to be obtained while the thermal conductivity has to be low.

Even if oxides are favorable for long-term operation at high temperatures due to the excellent chemical stability, weak toxicity, and oxidation resistance, they

* Corresponding author.
E-mail: fabiandelorme@yahoo.fr

were not considered as potential thermoelectric materials before the discovery of large Seebeck coefficient and power factor in the metallic oxide Na_xCoO_2 in 1997 [1]. Several other p-type layered cobalt oxides with high thermoelectric properties have been developed [2–11]. Other oxides, such as doped ZnO [12,13] or doped In_2O_3 [14,15], as well as several perovskite-type compositions ($CaMnO_3$ [16], $SrTiO_3$ [17], and more recently (K,Na)NbO_3 [18] or $Ba_{6-3x}Nd_{8+2x}Ti_{18}O_{54}$ [19]) have also presented promising properties.

$LaCoO_3$ compound has been studied for its high p-type thermoelectric properties at room temperature [20–23] but also for other numerous applications such as solid oxide fuel cells, oxygen separation membranes, catalysts, lasers, and sensors [24–26]. Substitution of La^{3+} by alkaline earth divalent ions such as Ca^{2+}, Sr^{2+}, and Ba^{2+} in $LaCoO_3$ enhances its electric and magnetic properties [27,28]. Indeed, these substitutions have a significant influence on oxygen vacancy concentration and/or crystal structure distortion in the material and are known to change the spin state of the Co^{3+} and Co^{4+} ions [21,27–35].

Controversial results have been published related to the thermoelectric properties of this material. Polycrystalline $La_{0.95}Sr_{0.05}CoO_3$ was first reported to have a high ZT value of 0.18 and S = 710 μV/K at room temperature [20], whereas more recent studies have found significantly lower thermopower values for this composition at the same temperature. For instance, Zhang *et al.* [36], Kozuka *et al.* [37], and Papageorgiou *et al.* [38] have reported that S is about 250 μV/K. However, high ZT value of 0.19 has still been reported with S = 213 μV/K for $La_{0.9}Sr_{0.1}CoO_3$ nanowires [22]. In a very recent paper, Singh and Pandey [39] reported a high Seebeck coefficient value of S = 635 μV/K at 300 K for $LaCoO_3$. Such differences could be related to the microstructure and/or synthesis route.

Therefore, as reported results are contradictory, the aim of this paper is to study the thermoelectric properties of $La_{1-x}Sr_xCoO_3$ ceramics. Moreover, the thermoelectric properties of ceramics with a cubic perovskite structure and $x > 0.8$ have never been investigated [37] whereas according to Koshibae *et al.* [40], they should present high n-type thermoelectric properties.

2 Materials and methods

$La_{1-x}Sr_xCoO_3$ ($0 \leqslant x \leqslant 1$) samples were prepared by conventional solid state reaction. The precursor La_2O_3 (Sigma Aldrich, purity ⩾ 99%), Co_3O_4 (Sigma Aldrich), and $SrCO_3$ (Sigma Aldrich, purity ⩾ 99.9%) were mixed in the stoichiometric ratio for 5 min at 400 rpm in an agate ball mill (Retsch PM 100).

Thermal pretreatment of the precursor La_2O_3 was necessary to remove any trace of lanthanum hydroxide ($La(OH)_3$). This pretreatment was carried out at 800 ℃ for 2 h. A plausible explanation for the presence of $La(OH)_3$ may be the hydration originated from air.

Only for $0.9 < x \leqslant 1$, a slight amount of silicon (Sigma Aldrich, purity ⩾ 99%) was added to the reaction mixture. Indeed, Kozuka *et al.* [37] have shown that the perovskite structure is not stable for such high substitution rates, but Hancock and Slater [41] have shown that the cubic perovskite structure can be stabilized by substituting 3% cobalt by silicon.

The powders of $La_{1-x}Sr_xCoO_3$ ($0 \leqslant x \leqslant 0.9$) were pelletized with a small amount of PVA (5% weight) as binder. To avoid any contamination, the pellets were placed on $LaCoO_3$ previously sintered pellets deposited on zirconia beads in an alumina crucible (Fig. 1). They were calcined at 1273 K for 12 h in air with a heating rate of 5 K/min, and slowly cooled down. This step has been repeated twice after manual grinding. Finally, the calcined samples were pressed into pellets, and sintered for 12 h in air at 1673 K for $0 \leqslant x \leqslant 0.7$ and at 1473 K for x = 0.8. For the powders of $La_{1-x}Sr_xCo_{0.97}Si_{0.03}O_3$ ($0.9 \leqslant x \leqslant 1$), the last sintering was realized at only 1373 K for 12 h in air to avoid transformation into brownmillerite.

The samples thus obtained were characterized by X-ray powder diffraction (XRD) on a BRUKER D8 diffractometer using Cu Kα radiation (λ = 1.5418 Å) and operating at 40 kV and 40 mA at room temperature. The patterns have been recorded from 5° to 85° (2θ) with a step of 0.02° and acquisition time of 2 s per step. The lattice parameters were refined by the Rietveld

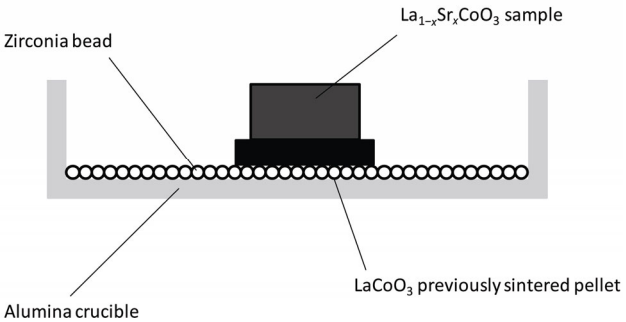

Fig. 1 Schematic representation of the synthesis set-up.

method using the Fullprof software [42]. Oxygen content in $La_{1-x}Sr_xCoO_3$ samples was determined by iodometric titration [43,44].

Electrical conductivity and Seebeck coefficient were simultaneously measured in ZEM III equipment (ULVAC Technologies) from 323 to 1000 K. The thermal diffusivity measurement of all specimens was carried out three times at each temperature in air from room temperature to 1000 K (Netzsch LFA 457). The heat capacity of the materials was measured from room temperature to 1073 K, with a heating rate of 20 ℃/min in platinum crucibles with alumina liners in argon atmosphere, using differential scanning calorimetry (Netzsch Pegasus 404 F1).

Apparent density of the samples was calculated from the weight and dimensions of the bars cut from the pellets for ZEM-3 characterization and the theoretical value [45].

The scanning electron microscopy (SEM) observations have been performed using FEI Quanta 200 microscope coupled with an energy dispersive spectrometer (EDS, Oxford INCA X-Act) without prior coating of the samples.

3 Results and discussion

XRD patterns registered at room temperature (Fig. 2) confirm $La_{1-x}Sr_xCoO_3$ perovskite pure phase formation over the whole composition range of the solid solution ($0 \leqslant x \leqslant 1$). According to Kozuka *et al.* [37], beside perovskite phase, for $x = 0.9$ in air, a secondary brownmillerite phase ($Sr_2Co_2O_5$) is obtained and for $x = 1$, a single brownmillerite phase is synthesized. However, as shown in Fig. 2, the substitution of 3% cobalt by silicon allows to reach a single cubic perovskite phase for $x = 0.9$, 0.95, and 1. Therefore, the whole $La_{1-x}Sr_xCoO_3$ solid solution from $x = 0$ to 1 has been stabilized.

The results of the refined structural parameters show a phase transition depending on the Sr concentration. XRD patterns show a gradual transition from rhombohedral to cubic perovskite phase (Fig. 2). For the low values of x, this phase transition is mainly manifested by the doubling of the diffraction peaks located at 32°, 40°, 52°, and 68° of 2θ. Figure 3 illustrates the Rietveld refinement for representative samples of the two phases, rhombohedral and cubic perovskite. For $0 \leqslant x \leqslant 0.5$, the diffraction patterns are indexed in a rhombohedral system ($LaCoO_3$ PDF Card No. 48-0123 [45]) with $R\bar{3}c$ space group (Fig. 3(a)). The unit cell parameters are about $a_h \approx 5.43$ Å and $c_h \approx 13.15$ Å. However, the patterns for the sintered samples with $0.5 < x \leqslant 1$ are indexed in a cubic structure ($Pm\bar{3}m$ space group) (Fig. 3(b)). The unit cell parameter is close to $a \approx 3.83$ Å ($SrCoO_3$ PDF Card No. 38-1148 [46]).

Figure 4 shows the lattice parameters as a function of x. In the rhombohedral system, for $0 \leqslant x \leqslant 0.5$, a and b parameters increase up to $x \leqslant 0.15$, and reduce for $x > 0.15$. However, c lattice parameter increases with increase in x. Thus, for this concentration range, the substitution of Sr^{2+} cations has more effects on cell parameter c than on cell parameter a. This result points out that the unit cell elongates along the c-axis with increasing cation substitution content. This lattice parameter variation is similar to that observed in $La_{1-x}Sr_xCoO_3$ obtained in previous works [47–49]. The

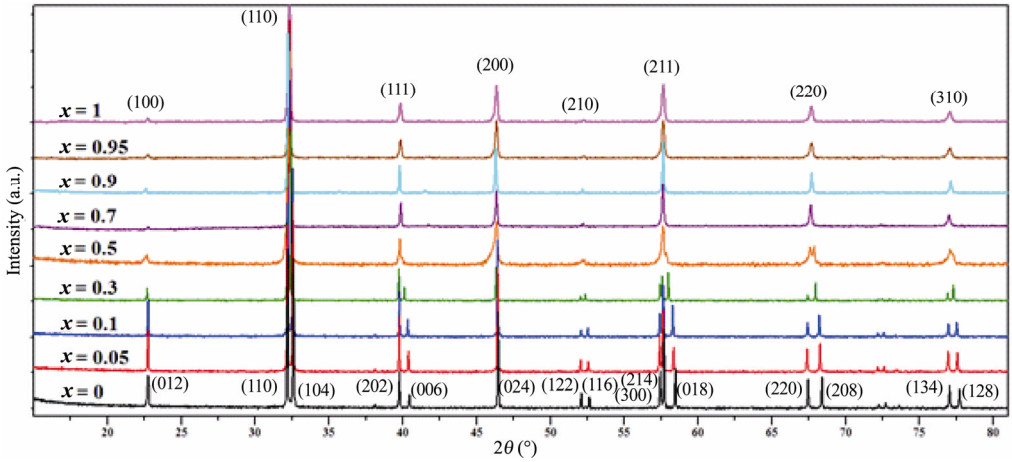

Fig. 2 XRD patterns of the $La_{1-x}Sr_xCoO_3$ solid solution at room temperature with $0 \leqslant x \leqslant 1$.

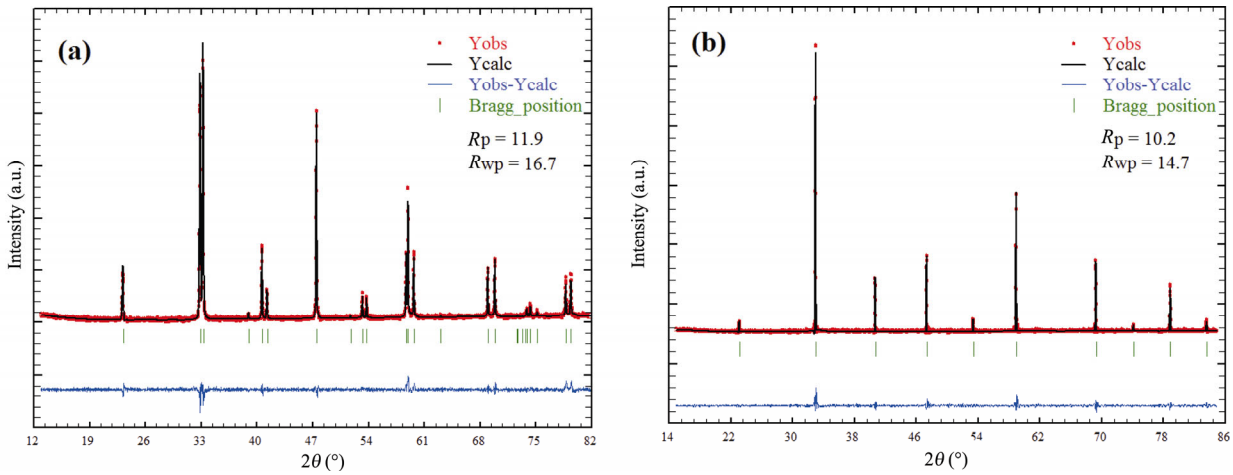

Fig. 3 Rietveld refinement results of XRD patterns for (a) $La_{0.95}Sr_{0.05}CoO_3$ and (b) $La_{0.3}Sr_{0.7}CoO_3$. The experimental data are shown as dots; the global fitting profile and the difference curve are shown as solid lines; the calculated reflection positions are indicated by stick marks.

plot of the *c*/*a* ratio is shown in Fig. 4 to confirm that substitutions are successful [12]. On the other hand, in the cubic symmetry, for $x \geqslant 0.7$, the lattice parameter of the *a*-axis linearly increases with increasing Sr substitution. Since the ionic radius of La^{3+} (0.136 nm [50]) is smaller than that of Sr^{2+} (0.144 nm [50]), it confirms the incorporation of Sr ions in the $LaCoO_3$ lattice. However, the charge neutrality in the solid solution is maintained, when the sample is substituted with Sr element, by increasing the oxygen vacancy concentration and/or the transition of the valence of Co cations from Co^{3+} to Co^{4+} [51–53]. Since both ionic radii of Co^{4+} and Co^{3+} are very close, 0.0545 and 0.053 nm, respectively [21], it cannot make a significant contribution to the lattice parameters. However, an additional expansion of the crystal lattice caused by the presence of oxygen vacancies in the ionic sublattice can occur. Indeed, these oxygen vacancies induce a Coulomb repulsion between neighboring cations [21,52].

Indeed, in order to determine the oxygen content of the different samples and degree of cobalt oxidation, we proceeded to iodometric titration. Figure 5 shows the valence of cobalt and the oxygen content ($3\pm\delta$) as a function of *x*. For low values of *x*, the samples are stoichiometric with δ values close to 0. For $x > 0.15$, the oxygen content decreases with increasing Sr content. Therefore, the mixed valence of cobalt increases as a function of *x*, with a slope change for $x > 0.15$. These results of the valence of cobalt and the oxygen content as a function of *x* are similar to the previous studies estimated by various methods such as iodometric titration, Rietveld refinement, and thermogravimetric analysis [37,47,49,54,55]. Nevertheless, for *x* values greater than 0.9, a discontinuity in the variation of the content and mixed cobalt valence is observed. This phenomenon can be related to synthesis protocol change.

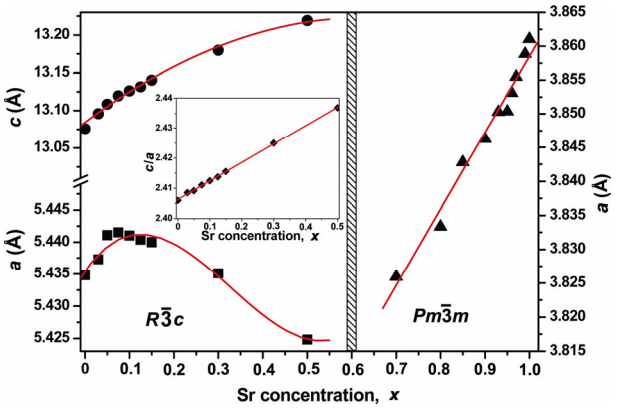

Fig. 4 Variation of lattice parameters as a function of *x* in $La_{1-x}Sr_xCoO_3$.

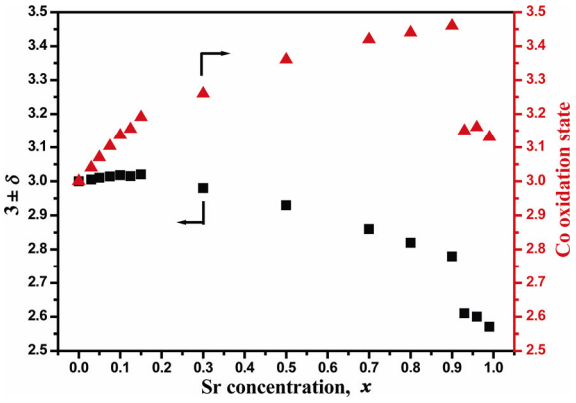

Fig. 5 Variation of the oxygen content ($3\pm\delta$) and the average valence of cobalt as a function of Sr concentration in $La_{1-x}Sr_xCoO_{3\pm\delta}$ with $0 \leqslant x \leqslant 1$ at 323 K.

Figure 6 displays the morphology of the microcrystalline sample observed by scanning electron microscopy. For ceramics densified at a temperature of about 1673 K ($x \leqslant 0.7$), the SEM micrographs reveal a little inter-granular porosity observed at triple points. Indeed, the porosity is eliminated by the notable granular growth with a grain size up to 50 μm. As an example, the micrograph of $La_{0.95}Sr_{0.05}CoO_3$ sample is presented in Fig. 6(a). These ceramics have high relative density ($\approx$ 94%) [45]. However, for $La_{1-x}Sr_xCoO_3$ samples densified at temperatures below 1473 K ($x \geqslant 0.8$), Fig. 6(b) corresponding to the $La_{0.2}Sr_{0.8}CoO_3$ sample shows the presence of inter- and intra-granular porosities. Under this sintering condition, the granular growth is more limited with a grain size not exceeding 20 μm. The samples have reached a relative density between 77% and 87% of the theoretical density. Chemical compositions obtained by EDS are homogeneous and consistent with the theoretical compositions.

The study of the electrical properties of cobaltites ($La_{1-x}Sr_xCoO_3$) was carried out by a simultaneous measurement of the electrical conductivity and the Seebeck coefficient at 330 K (Fig. 7). Measurements of the electrical conductivity (Fig. 7(a)) show that the ceramics substituted by Sr exhibit a high electric conductivity at low temperatures. The curve of the electrical conductivity σ versus the substitution rate x presents an optimum value for $x = 0.3$ with a value of $\sigma_{max} \approx 3\times10^5$ S·m^{-1} at 330 K. The variation of the electrical conductivity can be correlated to the charge carrier density and the variation of the oxygen content. Indeed for $x < 0.3$, the increase of σ is accompanied by an increase of the mixed valence of cobalt and a decrease of the oxygen content. Similar variations in electrical conductivity were observed in previous studies with optimal values with similar order of magnitude: for Iwasaki *et al.* [54], $\sigma_{max} \approx 10^6$ S·m^{-1} for $x = 0.4$, for Wang *et al.* [21], $\sigma_{max} = 1.7\times10^5$ S·m^{-1} for $x = 0.3$, and for Kozuka *et al.* [37], $\sigma_{max} = 4.4\times10^5$ S·m^{-1} for $x = 0.4$. For $0.9 < x \leqslant 1$, a slight increase in conductivity is observed. This increase may be related to the reduction of carrier concentration due to the decrease of the oxygen content, related to the slightly different synthesis process. Electrical conductivity

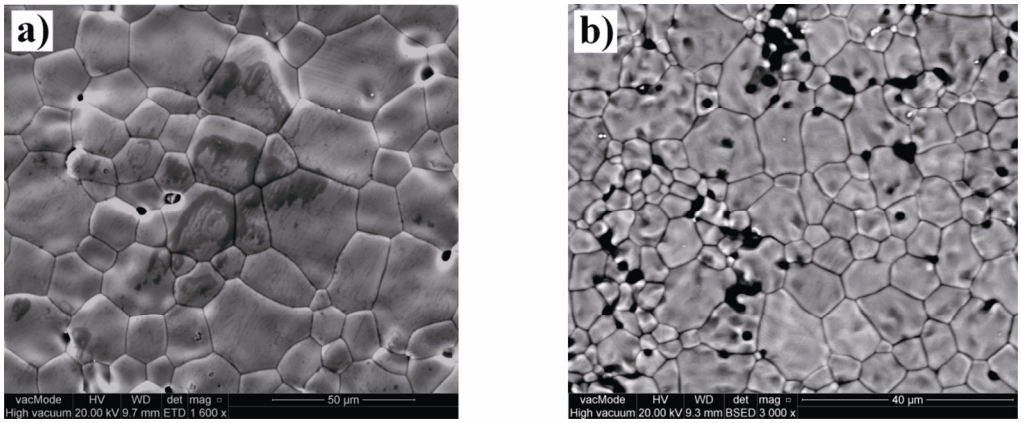

Fig. 6 SEM micrographs of (a) $La_{0.95}Sr_{0.05}CoO_3$ and (b) $La_{0.2}Sr_{0.8}CoO_3$ densified at 1673 K and 1473 K respectively.

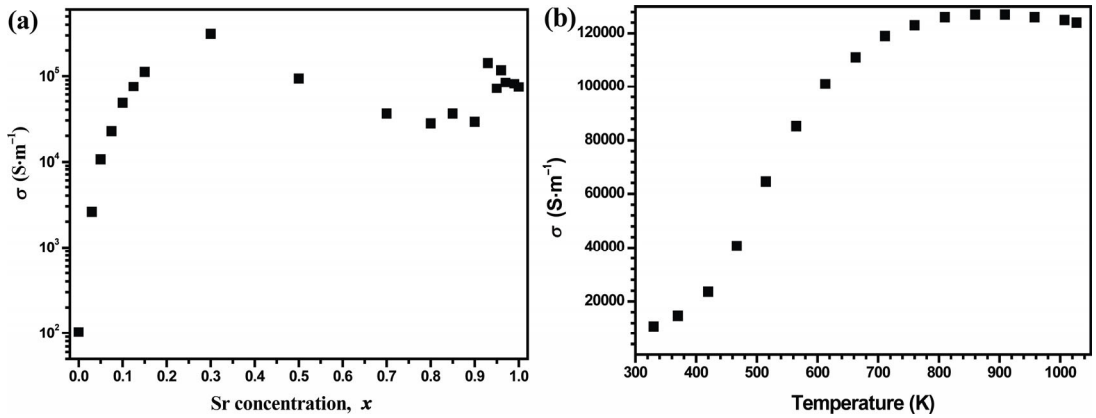

Fig. 7 Electrical conductivity (σ) for $La_{1-x}Sr_xCoO_3$ with (a) $0 \leqslant x \leqslant 1$ at 330 K and (b) $x = 0.05$ at different temperatures.

presents a conventional semiconductor behavior, i.e., it increases when temperature increases (Fig. 7(b)).

The variation of the Seebeck coefficient (Fig. 8(a)) as a function of the Sr concentration shows that at low temperature, for $x = 0$, S is negative (–250 μV/K), while for $x > 0$, S becomes positive. Then, it can be deduced that the substitution of La^{3+} by Sr^{2+}, even at low doping levels, leads to a change of carrier type. The highest value ($S = 270$ μV/K) is observed for $x = 0.05$. For $x > 0.05$, the Seebeck coefficient decreases when the Sr concentration increases. The decrease of the Seebeck coefficient (S) with increasing x shows that the carrier concentration increases as a function of x. This is consistent with the substitution of trivalent La^{3+} cations by divalent Sr^{2+} cations. Otherwise, for values of $x > 0.15$, we notice very low values of S, which indicates the metallic conductivity of samples. These S behaviors for $La_{1-x}Sr_xCoO_3$ samples were also observed in several previous studies [36–38,54,56]. With the exception of Androulakis *et al.* [20] who presented a value of $S = 710$ μV/K, this work and the most recent ones [37,57] show Seebeck coefficient values which remain lower than that of Androulakis *et al.* [20] and not exceeding 300 μV/K. Moreover, the Seebeck coefficient decreases when temperature increases (Fig. 8(b)). For $0.9 < x \leqslant 1$, a large negative Seebeck coefficient is not observed as expected by Koshibae *et al.*'s model [40]. This may be related to the decrease of the oxygen content: indeed, this leads to a cobalt average valence between 3.1 and 3.2, far away from the close to 4 value necessary to increase the Seebeck coefficient.

By combining the Seebeck coefficient and electrical conductivity, the dependence of power factor (PF) as a function of the Sr concentration for these samples is shown in Fig. 9. At low temperature, $La_{1-x}Sr_xCoO_3$ has a high PF. The optimal value is recorded at 330 K with a value of $PF_{max} = 3.11\times10^{-4}$ $W\cdot m^{-1}\cdot K^{-2}$ for $x = 0.05$.

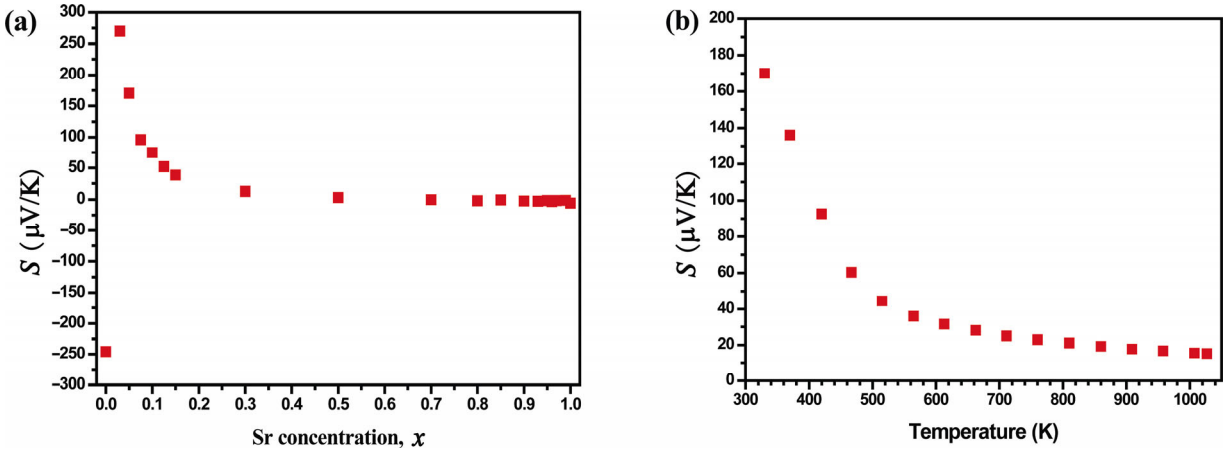

Fig. 8 Seebeck coefficient (S) for $La_{1-x}Sr_xCoO_3$ with (a) $0 \leqslant x \leqslant 1$ at 330 K and (b) $x = 0.05$ at different temperatures.

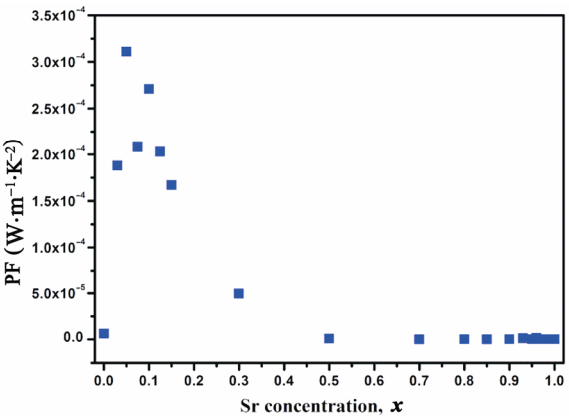

Fig. 9 Power factor (PF) for $La_{1-x}Sr_xCoO_3$ with $0 \leqslant x \leqslant 1$ at 330 K.

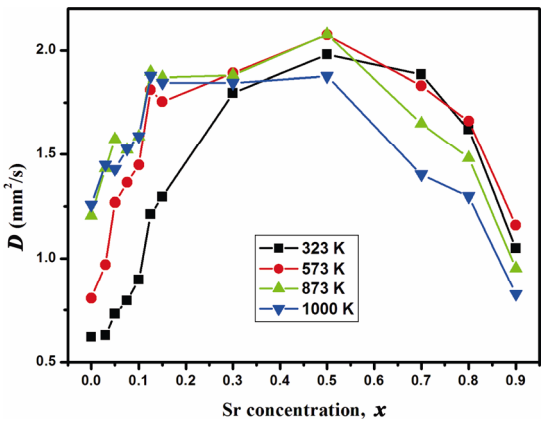

Fig. 10 Variation of thermal diffusivity as a function of x for $La_{1-x}Sr_xCoO_3$ with $0 \leqslant x \leqslant 1$ at 323, 573, 873, and 1000 K.

This result is lower than 18×10^{-4} W·m^{-1}·K^{-2} reported by Androulakis *et al.* [20] (x = 0.05 at 300 K) because of the large difference in the Seebeck coefficient. However, it is consistent with the more recent studies on $La_{1-x}Sr_xCoO_3$ [37,57].

Figure 10 shows the variation of thermal diffusivity as a function of the substitution rate for temperatures ranging from 323 to 1000 K. This figure shows that at low temperature and for low Sr concentration values, the thermal diffusivity is minimal (D = 0.6 mm^2/s at 323 K for x = 0.03). The thermal diffusivity increases with the Sr concentration to reach a maximum value when x = 0.5. This is due to the substitution of heavy lanthanum element by the lighter strontium element and also to the increase of the electrical conductivity. However, it decreases for values of x higher than 0.5. This decrease can be correlated to the structural change.

Figure 11 shows the thermal conductivity κ of $La_{1-x}Sr_xCoO_3$ samples as a function of temperature with x = 0, 0.05, and 0.1. The thermal conductivity (κ) has been calculated from the thermal diffusivity (D) and the specific heat capacity (C_p) as well as the density (d) according to equation: $\kappa = DC_pd$. Around room temperature, the thermal conductivity increases when the substitution rate increases. Indeed, this increase in thermal conductivity can be correlated with the increase in diffusivity when the substitution rate increases. On the other hand, it is noted that as the temperature increases, the thermal conductivity increases to reach a maximum value of 6.6 W·m^{-1}·K^{-1} for x = 0.05 at 900 K. Thermal conductivity reported for x = 0.05 is slightly higher than the ones reported by Androulakis *et al.* [20] and Zhou *et al.* [57] but consistent with the more recent one of Viskadourakis *et al.* [58].

Figure 12 shows the temperature dependence of the figure of merit ZT of the $La_{1-x}Sr_xCoO_3$ sample with x = 0, 0.05, and 0.1. The figure of merit (ZT) shows a maximum value of 0.039 for x = 0.05 at 323 K and rapidly decreases when the temperature increases. Decrease in ZT as a function of temperature is attributed to both the decrease in the Seebeck coefficient (S) and increase in thermal conductivity (κ). On the other hand, the value is lower than the 0.18 value (x = 0.05 at 300 K) reported by Androulakis *et al.* [20] because of the difference in the Seebeck coefficient (S) as mentioned above. However, it is consistent with more recent studies on $La_{1-x}Sr_xCoO_3$ [57,58].

4 Conclusions

In this work, we synthesized perovskite ceramics of the whole $La_{1-x}Sr_xCoO_3$ solid solution, from $0 \leqslant x \leqslant 1$ for the first time. The synthesis was carried out by solid state reaction. After several thermal cycles, pure and dense ceramics are obtained, over the whole composition range. The characterization by XRD shows a structural change for x = 0.5. The electrical and thermal properties show important variations depending on x: the electrical conductivity exhibits an optimum for x = 0.3 ($\sigma_{max} \approx 3\times10^5$ S·m^{-1}), while the Seebeck coefficient decreases as x increases and presents anoptimum value for x = 0.05. This leads to optimum electrical properties for x = 0.05 at 330 K with PF_{max} = 3.11×10^{-4} W·m^{-1}·K^{-2}. The thermal diffusivity is increasing with temperature and also when x increases

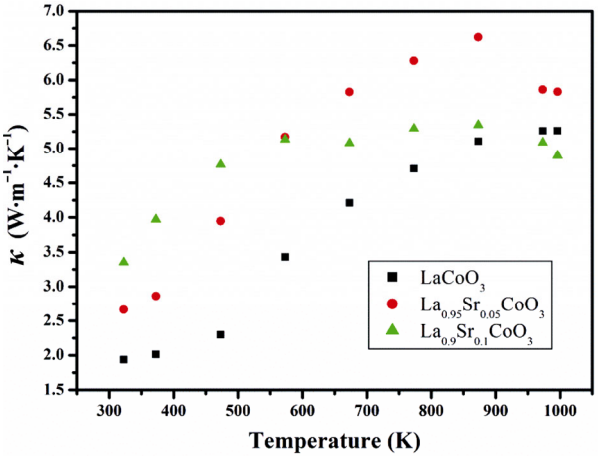

Fig. 11 Temperature dependence of the thermal conductivity of the $La_{1-x}Sr_xCoO_3$ sample with x = 0, 0.05, and 0.1.

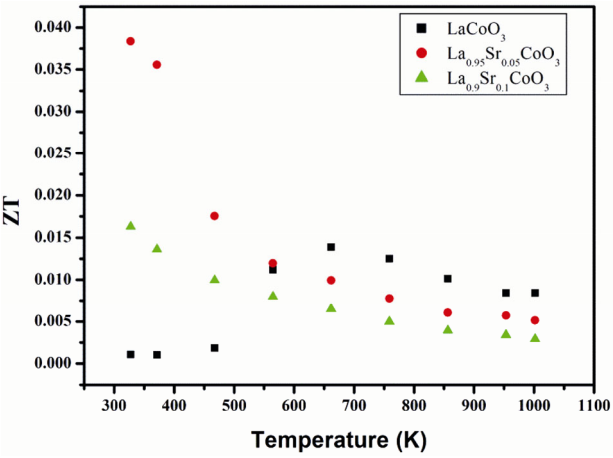

Fig. 12 Temperature dependence of the ZT value of the $La_{1-x}Sr_xCoO_3$ sample with x = 0, 0.05, and 0.1.

up to 0.5. For $x = 0.05$, this study is consistent with the value recently published by Kozuka *et al.* [37] rather than with the first high ZT value reported by Androulakis *et al.* [20]. As the highest power factor is reached at low temperature as well as the lowest thermal conductivity, $La_{1-x}Sr_xCoO_3$ compounds with low x values appear as very promising thermoelectric materials around room temperature, on the contrary to layered cobalt oxides. However, for high x values, the Seebeck coefficient values close to zero make these materials not suitable for thermoelectric applications, except if their oxygen content could be increased.

Acknowledgements

The authors acknowledge ADEME (Agence de l'Environnement et de la Maîtrise de l'Energie) and Plan d'Investissment d'Avenir PIA "Tours 2015" for the financial support.

References

[1] Terasaki I, Sasago Y, Uchinokura K. Large thermoelectric power in $NaCo_2O_4$ single crystals. *Phys Rev B* 1997, **56**: R12685.

[2] Li S, Funahashi R, Matsubara I, *et al*. High temperature thermoelectric properties of oxide $Ca_9Co_{12}O_{28}$. *J Mater Chem* 1999, **9**: 1659–1660.

[3] Masset AC, Michel C, Maignan A, *et al*. Misfit-layered cobaltite with an anisotropic giant magnetoresistance: $Ca_3Co_4O_9$. *Phys Rev B* 2000, **62**: 166.

[4] Delorme F, Fernandez Martin C, Marudhachalam P, *et al*. Effect of Ca substitution by Sr on the thermoelectric properties of $Ca_3Co_4O_9$ ceramics. *J Alloys Compd* 2011, **509**: 2311–2315.

[5] Delorme F, Ovono Ovono D, Marudhachalam P, *et al*. Effect of precursors size on the thermoelectric properties of $Ca_3Co_4O_9$ ceramics. *Mater Res Bull* 2012, **47**: 1169–1175.

[6] Diez JC, Torres MA, Rasekh Sh, *et al*. Enhancement of $Ca_3Co_4O_9$ thermoelectric properties by Cr for Co substitution. *Ceram Int* 2013, **39**: 6051–6056.

[7] Chen C, Zhang T, Donelson R, *et al*. Thermopower and chemical stability of $Na_{0.77}CoO_2/Ca_3Co_4O_9$ composites. *Acta Mater* 2014, **63**: 99–106.

[8] Delorme F, Diaz-Chao P, Guilmeau E, *et al*. Thermoelectric properties of $Ca_3Co_4O_9$–Co_3O_4 composites. *Ceram Int* 2015, **41**: 10038–10043.

[9] Funahashi R, Shikano M. $Bi_2Sr_2Co_2O_y$ whiskers with high thermoelectric figure of merit. *Appl Phys Lett* 2002, **81**: 1459–1461.

[10] Yamauchi H, Sakai K, Nagai T, *et al*. Parent of misfit-layered cobalt oxides: $[Sr_2O_2]_qCoO_2$. *Chem Mater* 2006, **18**: 155–158.

[11] Delorme F, Chen C, Pignon B, *et al*. Promising high temperature thermoelectric properties of dense $Ba_2Co_9O_{14}$ ceramics. *J Eur Ceram Soc* 2017, **37**: 2615–2620.

[12] Ohtaki M, Araki K, Yamamoto K. High thermoelectric performance of dually doped ZnO ceramics. *J Electron Mater* 2009, **38**: 1234–1238.

[13] Díaz-Chao P, Giovannelli F, Lebedev O, *et al*. Textured Al-doped ZnO ceramics with isotropic grains. *J Eur Ceram Soc* 2014, **34**: 4247–4256.

[14] Bérardan D, Guilmeau E, Maignan A, *et al*. In_2O_3:Ge, a promising n-type thermoelectric oxide composite. *Solid State Commun* 2008, **146**: 97–101.

[15] Guilmeau E, Bérardan D, Simon Ch, *et al*. Tuning the transport and thermoelectric properties of In_2O_3 bulk ceramics through doping at in-site. *J Appl Phys* 2009, **106**: 053715.

[16] Flahaut D, Mihara T, Funahashi R, *et al*. Thermoelectrical properties of A-site substituted $Ca_{1-x}Re_xMnO_3$ system. *J Appl Phys* 2006, **100**: 084911.

[17] Muta H, Kurosaki K, Yamanaka S. Thermoelectric properties of rare earth doped $SrTiO_3$. *J Alloys Compd* 2003, **350**: 292–295.

[18] Delorme F, Bah M, Schoenstein F, *et al*. Thermoelectric properties of oxygen deficient $(K_{0.5}Na_{0.5})NbO_3$ ceramics. *Mater Lett* 2016, **162**: 24–27.

[19] Azough F, Freer R, Yeandel SR, *et al*. $Ba_{6-3x}Nd_{8+2x}Ti_{18}O_{54}$ tungsten bronze: A new high-temperature n-type oxide thermoelectric. *J Electron Mater* 2016, **45**: 1894–1899.

[20] Androulakis J, Migiakis P, Giapintzakis J. $La_{0.95}Sr_{0.05}CoO_3$: An efficient room-temperature thermoelectric oxide. *Appl Phys Lett* 2004, **84**: 1099–1101.

[21] Wang Y, Sui Y, Ren P, *et al*. Correlation between the structural distortions and thermoelectric characteristics in $La_{1-x}A_xCoO_3$ (A = Ca and Sr). *Inorg Chem* 2010, **49**: 3216–3223.

[22] Wang Y, Fan HJ. Improved thermoelectric properties of $La_{1-x}Sr_xCoO_3$ nanowires. *J Phys Chem C* 2010, **114**: 13947–13953.

[23] Li F, Li J-F. Effect of Ni substitution on electrical and thermoelectric properties of $LaCoO_3$ ceramics. *Ceram Int* 2011, **37**: 105–110.

[24] Kharton VV, Figueiredo FM, Kovalevsky AV, *et al*. Processing, microstructure and properties of $LaCoO_{3-\delta}$ ceramics. *J Eur Ceram Soc* 2001, **21**: 2301–2309.

[25] Deac IG, Vladescu A, Balasz I, *et al*. Low temperature magnetic properties of $Pr_{0.7}(Ca,Sr)_{0.3}CoO_3$ oxides. *Acta Phys Pol A* 2011, **120**: 306–310.

[26] Li F, Li J-F. Enhanced thermoelectric performance of separately Ni-doped and Ni/Sr-codoped $LaCoO_3$ nanocomposites. *J Am Ceram Soc* 2012, **95**: 3562–3568.

[27] Masuda H, Fujita T, Miyashita T, *et al*. Transport and magnetic properties of $R_{1-x}A_xCoO_3$ (R = La, Pr and Nd; A = Ba, Sr and Ca). *J Phys Soc Jpn* 2003, **72**: 873–878.

[28] Muta K, Kobayashi Y, Asai K. Magnetic, electronic transport, and calorimetric investigations of $La_{1-x}Ca_xCoO_3$ in comparison with $La_{1-x}Sr_xCoO_3$. *J Phys Soc Jpn* 2002,

71: 2784–2791.

[29] Kun R, Populoh S, Karvonen L, *et al*. Structural and thermoelectric characterization of Ba substituted $LaCoO_3$ perovskite-type materials obtained by polymerized gel combustion method. *J Alloys Compd* 2013, **579**: 147–155.

[30] Kozuka H, Yamagiwa K, Ohbayashi K, *et al*. Origin of high electrical conductivity in alkaline-earth doped $LaCoO_3$. *J Mater Chem* 2012, **22**: 11003–11005.

[31] Sánchez-Andújar M, Rinaldi D, Caciuffo R, *et al*. Magnetotransport properties of spin-glass-like layered compounds $La_{1-x}Sr_{1+x}CoO_4$. *Solid State Sci* 2006, **8**: 901–907.

[32] Raccah PM, Goodenough JB. A localized-electron to collective-electron transition in the system (La,Sr)CoO_3. *J Appl Phys* 1968, **39**: 1209.

[33] Señarís-Rodríguez MA, Goodenough JB. Magnetic and transport properties of the system $La_{1-x}Sr_xCoO_{3-\delta}$ ($0 < x \leqslant 0.50$). *J Solid State Chem* 1995, **118**: 323–336.

[34] Itoh M, Natori I, Kubota S, *et al*. Spin-glass behavior and magnetic phase diagram of $La_{1-x}Sr_xCoO_3$ ($0 \leqslant x \leqslant 0.5$) studied by magnetization measurements. *J Phys Soc Jpn* 1994, **63**: 1486–1493.

[35] Caciuffo R, Rinaldi D, Barucca G, *et al*. Structural details and magnetic order of $La_{1-x}Sr_xCoO_3$ ($x < \sim 0.3$). *Phys Rev B* 1999, **59**: 1068.

[36] Zhang X, Li XM, Chen TL, *et al*. Thermoelectric and transport properties of $La_{0.95}Sr_{0.05}CoO_3$. *J Cryst Growth* 2006, **286**: 1–5.

[37] Kozuka H, Yamada H, Hishida T, *et al*. Electronic transport properties of the perovskite-type oxides $La_{1-x}Sr_xCoO_{3\pm\delta}$. *J Mater Chem* 2012, **22**: 20217–20222.

[38] Papageorgiou C, Athanasopoulos GI, Kyratsi Th, *et al*. Influence of processing conditions on the thermoelectric properties of $La_{1-x}Sr_xCoO_3$ (x = 0, 0.05). *AIP Conf Proc* 2012, **1449**: 323.

[39] Singh S, Pandey SK. Understanding the thermoelectric properties of $LaCoO_3$ compound. *Philos Mag* 2017, **97**: 451–463.

[40] Koshibae W, Tsutsui K, Maekawa S. Thermopower in cobalt oxides. *Phys Rev B* 2000, **62**: 6869.

[41] Hancock CA, Slater PR. Synthesis of silicon doped $SrMO_3$ (M = Mn, Co): Stabilization of the cubic perovskite and enhancement in conductivity. *Dalton Trans* 2011, **40**: 5599–5603.

[42] Rodríguez-Carvajal J. Recent advances in magnetic structure determination by neutron powder diffraction. *Phys B: Condens Matter* 1993, **192**: 55–69.

[43] Nadalin RJ, Brozda WB. Chemical methods for the determination of the "oxidizing (or reducing) power" of certain materials containing a multivalent element in several oxidation states. *Anal Chim Acta* 1963, **28**: 282–293.

[44] Stevenson JW, Armstrong TR, Carneim RD, *et al*. Electrochemical properties of mixed conducting perovskites $La_{1-x}M_xCo_{1-y}Fe_yO_{3-\delta}$ (M = Sr, Ba, Ca). *J Electrochem Soc* 1996, **143**: 2722–2729.

[45] Closset NMLNP, van Doorn RHE, Kruidhof H, *et al*. About the crystal structure of $La_{1-x}Sr_xCoO_{3-\delta}$ ($0 \leqslant x \leqslant 0.6$). *Powder Diffr* 1996, **11**: 31–34.

[46] Bezdicka P, Wattiaux A, Grenier JC, *et al*. Preparation and characterization of fully stoichiometric $SrCoO_3$ by electrochemical oxidation. *Z Anorg Allg Chem* 1993, **619**: 7–12.

[47] Itoh T, Inukai M, Kitamura N, *et al*. Correlation between structure and mixed ionic–electronic conduction mechanism for $(La_{1-x}Sr_x)CoO_{3-\delta}$ using synchrotron X-ray analysis and first principles calculations. *J Mater Chem A* 2015, **3**: 6943–6953.

[48] Jiamprasertboon A, Okamoto Y, Hiroi Z, *et al*. Thermoelectric properties of Sr and Mg double-substituted $LaCoO_3$ at room temperature. *Ceram Int* 2014, **40**: 12729–12735.

[49] Mineshige A, Inaba M, Yao T, *et al*. Crystal structure and metal–insulator transition of $La_{1-x}Sr_xCoO_3$. *J Solid State Chem* 1996, **121**: 423–429.

[50] Shannon RD. Revised effective ionic radii and systematic studies of interatomic distances in halides and chalcogenides. *Acta Cryst* 1976, **A32**: 751–767.

[51] Maignan A, Hébert S, Pi L, *et al*. Perovskite manganites and layered cobaltites: Potential materials for thermoelectric applications. *Cryst Eng* 2002, **5**: 365–382.

[52] Li F, Li J-F, Li J-H, *et al*. The effect of Cu substitution on microstructure and thermoelectric properties of $LaCoO_3$ ceramics. *Phys Chem Chem Phys* 2012, **14**: 12213–12220.

[53] Bhatt HD, Vedula R, Desu SB, *et al*. $La_{1-x}Sr_xCoO_3$ for thin film thermocouple applications. *Thin Solid Films* 1999, **350**: 249–257.

[54] Iwasaki K, Ito T, Nagasaki T, *et al*. Thermoelectric properties of polycrystalline $La_{1-x}Sr_xCoO_3$. *J Solid State Chem* 2008, **181**: 3145–3150.

[55] Orikasa Y, Ina T, Nakao T, *et al*. X-ray absorption spectroscopic study on $La_{0.6}Sr_{0.4}CoO_{3-\delta}$ cathode materials related with oxygen vacancy formation. *J Phys Chem C* 2011, **115**: 16433–16438.

[56] Koumoto K, Funahashi R, Guilmeau E, *et al*. Thermoelectric ceramics for energy harvesting. *J Am Ceram Soc* 2013, **96**: 1–23.

[57] Zhou AJ, Zhu TJ, Zhao XB, *et al*. Fabrication and thermoelectric properties of perovskite-type oxide $La_{1-x}Sr_xCoO_3$ (x = 0, 0.1). *J Alloys Compd* 2008, **449**: 105–108.

[58] Viskadourakis Z, Athanasopoulos GI, Kasotakis E, *et al*. Effect of microstructure on the thermoelectric performance of $La_{1-x}Sr_xCoO_3$. *J Solid State Chem* 2016, **243**: 111–118.